



Inclusion of shape parameters increases the accuracy of 3D models for microplastics mass quantification



Hiraku Tanoiri^a, Haruka Nakano^{a,b}, Hisayuki Arakawa^a, Ricardo Shohei Hattori^a, Masashi Yokota^{a,*}

^a Tokyo University of Marine Science and Technology, Konan 4-5-7, Minato-ku, Tokyo 108-8477, Japan

^b Environmental Management Research Institute, National Institute of Advanced Industrial Science and Technology (AIST), 16-1 Onogawa, Tsukuba 395-8569, Japan

ARTICLE INFO

Keywords:
Microplastics
Quantification
Characterization
Image analysis
Mass estimation
Methodology

ABSTRACT

As microplastics may bring about adverse effects on living organisms, it is important to establish more precise quantification approaches to better understand their dynamics. One method to determine the concentration of microplastics is to estimate their mass using three-dimensional (3D) models, but its accuracy is not well known. In this study, we evaluated the shape of the particles and verified the accuracy of a 3D model-based mass estimation using samples from a tidal flat facing Tokyo Bay. The particle shape evaluation suggested that the microplastics were flat and irregular in shape; based on these data, we created two types of models to estimate their mass. As a result, an accuracy of mass estimation by our model was higher than other models that consider the slenderness and flatness of particles. The optimization of mass estimation methods based on 3D models may improve the reliability of microplastic evaluation in monitoring studies.

1. Introduction

Since plastics began to be widely used by the industry in 1950s their production has grown vertiginously, reaching almost 350 million tons in 2017 (Association of Plastics manufacturers, 2018). Along with this production, the discharge of plastics into natural environments have also increased; for instance it was estimated that about 4.8–12.7 million tons of plastics entered the ocean in 2010 (Jambeck et al., 2015). Most of the plastic materials, which consist mainly of huge organic polymers, are thought to enter into marine environments gradually as small particles, due to natural fragmentation caused by the physical action of waves and by ultraviolet rays from the sunlight. The particles with a diameter of 5 mm or less are classified as “microplastics” according to some authors (Barnes et al., 2009; Cózar et al., 2014; Horton and Dixon, 2018; Ivar Do Sul and Costa, 2014) and they can be categorized according to their polymer type, shape, and color (GESAMP, 2019). However, there are still many divergences in the criteria for microplastic classification as some researchers consider 1 mm or less to be within the definition; recycled fibers (e.g., Rayon) are also considered as microplastics according to authors. In this context, petroleum products of less than 5 mm are defined as microplastics.

In the recent years there have been a lot of concerns related to their impacts, since they have been found not only in marine environments but also inside the body of living organisms (Davidson and Dudas, 2016; Qu et al., 2018; Silva-Cavalcanti et al., 2017; Ushijima et al., 2018). In rearing experiments it was demonstrated that the ingestion of microplastics by living organisms can induce neurotoxicity in goby *Pomatoschistus microps* (Oliveira et al., 2013), emaciation in lugworm *Arenicola marina* (Besseling et al., 2013), and reduced reproductive ability in oyster *Crassostrea gigas* (Sussarellu et al., 2016). Therefore, due to concerns about the adverse effects of microplastics on marine organisms and possibly on human health, it is important to better understand the dynamics of microplastics in marine environment.

An important and fundamental process for accurate monitoring of impacts caused by microplastics depends on their adequate quantification. However, the different methodologies employed in the quantification make it difficult to perform comparative evaluations among data from different studies. While some have expressed the quantity of microplastics in terms of number of pieces per unit area, unit volume or unit weight (Corami et al., 2020; Lots et al., 2017; Pan et al., 2019; Rocha-Santos and Duarte, 2015), numerical simulations of microplastic distribution and dynamics (Siegfried et al., 2017; Wang et al., 2008) or

* Corresponding author at: Tokyo University of Marine Science and Technology, Konan 4-5-7, Minato-ku, Tokyo 108-8477, Japan.

E-mail addresses: go414andrelax@gmail.com (H. Tanoiri), nakano.hrk@aist.go.jp (H. Nakano), arakawa@kaiyodai.ac.jp (H. Arakawa), [\(R.S. Hattori\)](mailto:Hattori.fish@gmail.com), yokota@kaiyodai.ac.jp (M. Yokota).

toxicity tests on organisms under laboratory conditions (Oliveira et al., 2013; Sussarellu et al., 2016) have used mass concentration. For example, according to a field survey, the amount of suspended microplastics at the mouth of the Yangtze River was about 3.0×10^3 pcs/m³ (Zhao et al., 2014) but the numerical simulations estimated the amount of plastic entering the ocean from the Yangtze River (China) to be 3.3×10^5 t/year (Lebreton et al., 2017). Thus, it is difficult to evaluate the proportion of microplastics in the plastic litter flowing out of this river without converting the concentration values from these two-research due to discrepancies between the model and the actual results. Furthermore, the use of length and number for quantitative expression of microplastics has been considered as inappropriate because they have three-dimensions (3D) and accidental fragmentation may occur during sample processing and analysis (Simon et al., 2018). Such fragmentation, in turn, can cause underestimation of the size and overestimation of the number of pieces. With this regard, since the mass of particles does not change even upon fragmentation, the use of mass concentration, in addition to length and number, may be more suitable for quantification of microplastics.

To measure the mass or volume of particles (including non-microplastics) in marine environments, the following methods have been used: measuring mass by pyr-GC/MS (Dierkes et al., 2019; Funck et al., 2020; Peters et al., 2018) or collection of suspended particulate matter on a filter for the determination of total mass. In case of volume, the determination from electrical resistance using a Coulter counter (Eisma, 1991; Uncles et al., 2006) and analysis of the 3D structure using optical interference technology (Bianco et al., 2020; Nayak et al., 2021; Takahashi et al., 2020).

One of the methods to estimate the mass of microplastics comprises the 3D model using the length of the particles (Cózar et al., 2014; Isobe et al., 2019; Simon et al., 2018). However, the similarity between these models shapes and the actual particle shapes and the accuracy of the estimated mass based on these models have not been clarified. Primpke et al. (2020a) reported that the method of simPLE (Primpke et al., 2020b), which introduced the mass estimation model of (Simon et al., 2018), was used for microplastics in sediments and surface waters of the southern North Sea, resulting a seven times mass overestimation of compared to the method using pyr-GC/MS. Thus, it is important to verify the accuracy of the mass estimation by the 3D models. In this context, this study aimed to establish a 3D-based model to increase the accuracy of mass quantification of microplastics. For this, we first clarified the

particle shape of microplastics by several indices. In addition, we investigated the relationship among shape, polymer type, and color in order to find out possible relationships or trends in our samples. Then we developed a model for estimating the mass of microplastics considering shape-related parameters. Finally, using samples from a tidal flat facing Tokyo Bay, the accuracy of this method was clarified and compared with that of models used in previous studies (Cózar et al., 2014; Isobe et al., 2019; Simon et al., 2018).

2. Material & Methods

2.1. Sampling

Samples were collected on June 4, 2020, at a tidal flat located at the mouth of Tsurumi River ($35^{\circ}29'51.2''N$, $139^{\circ}40'34.6''E$, Tokyo Bay, Japan, Fig. 1). This place was chosen because Tsurumi River passes through one of the most densely populated area in Japan (basin area: 235 km^2 , population density: about 9.2×10^3 people/km², MLITJapan, 2010, last access: 2/10/2021), and, consequently, the concentration and diversity of microplastics are estimated to be high (Kataoka et al., 2019). A rectangular frame of 1.0 m parallel to the coastline and 0.5 m perpendicular to the coastline was set up at an arbitrary point in the tidal zone. All drifted materials inside the frame were collected and transferred to the laboratory. A total of 351 particles of “large microplastics” measuring 1 mm to 5 mm in length (see Table 10. 10 in GESAMP, 2019) were randomly selected under a stereomicroscope and classified into five shapes (Fragment, Foam, Film, Line, and Pellet), based on the classification chart proposed by GESAMP (2019). In order to prevent the contamination of plastic particles, all equipment and instruments for sample collection and processing were cleaned prior to use.

2.2. Sample pretreatment and validation

Since a large number of shells were found at the sampling site, samples were initially treated with a 20% formic acid (HCOOH) solution for 10 min at room temperature for calcium carbonate removal. Then samples received a treatment with a solution of hydrogen peroxide (H_2O_2) and iron (II) sulfate heptahydrate ($FeSO_4 \cdot 7H_2O$, 0.01 g per 10 mL of 30% H_2O_2 , acidic condition of 0.5% HCOOH) for 3 days at room temperature, followed by another treatment with 20% potassium hydroxide solution (KOH) for 2 days at 50 °C. Finally, samples were rinsed

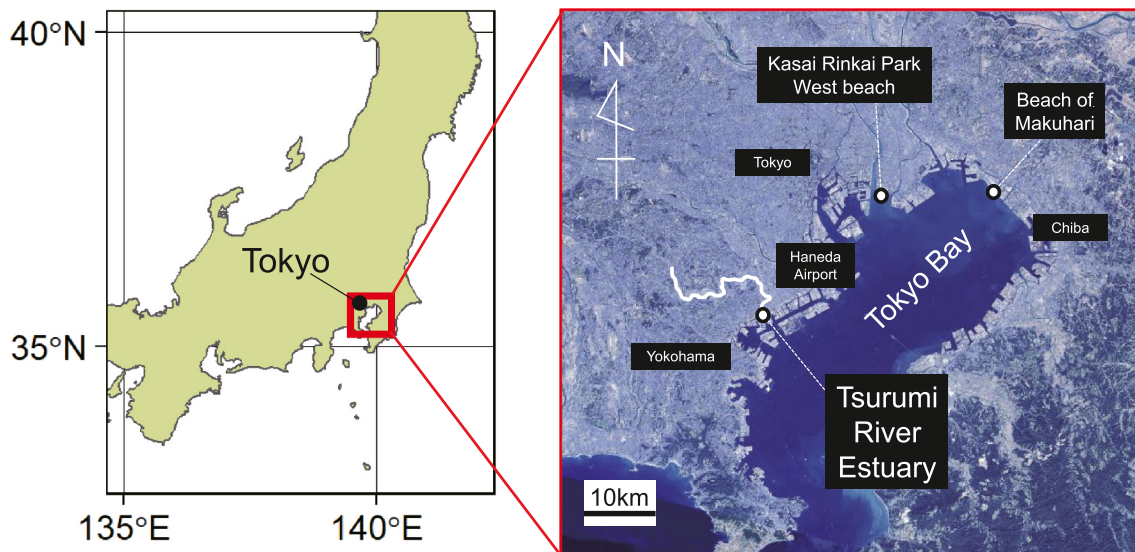


Fig. 1. Geographic map of Japan main Island with the sampling location and Tsurumi river. Created by processing Geospatial Information Authority of Japan website. (URL: <https://maps.gsi.go.jp/#5/36.104611/140.084556/&base=std&ls=std&disp=1&vs=c1j0h0k0l0u0t0z0r0s0m0f1>, data source: Landsat8 image (GSI, TSIC,GEO Grid/AIST), Landsat8 image (courtesy of the U.S. Geological Survey), submarine topography (GEBCO), last access: 2/11/2021).

with distilled water and dried at 50 °C for 1 day. These chemical treatments were performed according to Munno et al. (2018) and Ushijima et al. (2018).

Since previous studies on microplastic extraction methods have pointed out that the use of strong acids in chemical treatments and heating above 60 °C can cause loss or dissolution of microplastics (Claessens et al., 2013; Dehaut et al., 2016; Enders et al., 2017; Munno et al., 2018), this study used formic acid, a weak acid, in order to minimize the impacts on microplastics. The effects of this acid were compared by microscope images and mass measured before and after the treatment.

2.3. Sample analysis

The mass ($m[\text{g}]$) of the samples was measured using a precision balance (GR-202, A and D Corporation, Japan, accuracy $1.0 \times 10^{-4} \text{ g}$). Images (light source: dark field illumination method, with SZX2-ILST LED illumination mount, Olympus, Japan, exposure time: 27.8 ms, ISO: 400, $5.44 \times 10^3 \text{ dpi}$) were then captured using a binocular stereomicroscope (SZX10, Olympus, Japan) coupled with a camera (DP73, Olympus, Japan). Samples were also categorized into 17 colors (Red, Orange, Yellow, Chartreuse green, Green, Spring green, Cyan, Azure, Blue, Violet, Magenta, Rose based on the ISCC-NBS System of Color Designation recommended by GESAMP (2019), plus Clear, Opaque (Non-pigmented), White, Gray, and Black).

The length of the samples was measured using ImageJ (version 1.53a; Java 1.8.0_112). After converting the sample photos into black-and-white binary images, the area ($S[\text{cm}^2]$), the perimeter ($L_p[\text{cm}]$), the major axis diameter ($\phi_l[\text{cm}]$), and the minor axis diameter ($\phi_s[\text{cm}]$) of the approximate ellipse with area equal to S , were measured for all samples. In this study, the particle diameter ($\phi[\text{cm}]$) was defined as the average value of ϕ_l and ϕ_s values:

$$\phi = \frac{\phi_l + \phi_s}{2} \quad (1)$$

Component analysis of the sample was performed using Attenuated Total Reflection method (ATR method) by Fourier transform infrared spectrometer (FT-IR, IRT-6600, Jasco Corporation, Japan). The infrared absorption spectra at wavenumber 400–4000 cm^{-1} was measured and compared with the spectra in the KnowItAll library (Bio-Rad Laboratories, U.S.A) to identify the polymer type. At this time, samples that were judged not to be plastic based on their composition were excluded. The density (ρ) of the particles was determined from the identified polymer types (Table S 1). Foam was considered as Expanded plastic (GESAMP, 2019) and set to $\rho = 0.10$ regardless of the polymer type.

2.4. Evaluation of particle shape

It is important to understand the particle shape of microplastics in order to create accurate models. However, the shape classification of microplastics by GESAMP guidelines is done without clear standardization for classifications. In this study, we used a qualitative index based on Krumbein's roundness chart (Krumbein, 1941), which is the most widely used index for particle shape evaluation, and also two quantitative indexes for shape (Sugimoto et al., 1989).

The qualitative evaluation of particle shape was performed by converting the projected image to a Krumbein's Roundness index (R_K) using Takashimizu and Iiyoshi (2016)'s transformation formula. The transformation first calculate the corrected Roundness (R), an index proposed by Takashimizu and Iiyoshi (2016) using several particle parameters (See Supplemental Files p. 4 and Fig. S 1 for details on conversion). Originally, R_K was sought visually, and there is no clear basis for the classification criteria, but R and R_K have been shown to regress to a quadratic function with downward convexity, so that R_K can be objectively derived from the particle shape parameters. The value of R_K can then be replaced by a qualitative expression using Blott and Pye's (2008)

classification criteria: "Angular" ($0.0 < R_K < 0.13$), "Sub-angular" ($0.13 \leq R_K < 0.25$), "Sub-rounded" ($0.25 \leq R_K < 0.50$), and "Rounded" ($0.50 \leq R_K \leq 1.0$). However, the relative minimum value of the regression equation for R and R_K is 0.67, and R_K increases as R decreases in the range of $R \leq 0.67$ so it contradicts the assumption that R and R_K are proportional. Therefore, the particles with $R \leq 0.67$ were classified as "Irregular" without using R_K .

The quantitative evaluation of the particle shape was performed as follows. The shape characteristics of the particles were evaluated by dividing them into two indices: 1) Roundness (δ), which is the characteristic of the slenderness of the particle based on the diameter of the same area circle (ϕ_C), and 2) Smoothness (ζ), which is the characteristic of the irregularity of the particle contour based on the perimeter of the approximate ellipse (L_E):

$$\delta = \frac{\phi_C}{\phi_l}, \quad (0.0 \leq \delta \leq 1.0) \quad (2)$$

$$\zeta = \frac{L_E}{L_p}, \quad (0.0 \leq \zeta \leq 1.0) \quad (3)$$

According to these formulae, the closer δ is to 1, the closer the particle aspect ratio is to 1, and the closer ζ is to 1, the closer the particle is to a smooth ellipse. δ is equal to the square of the reciprocal of the aspect ratio. In this study, particles with δ greater than or equal to 0.50 were classified as ellipses, those with δ less than 0.50 as rods, those with ζ greater than or equal to 0.50 as smooth surfaces, and those with ζ less than 0.50 as rough surfaces, according to relative evaluation standards based on these indices. Moreover, we preliminary checked the validity of the image resolution of the sample for particle shape evaluation by testing the change in the indices using different resolution images of the same particles. As a result, we concluded that 1000 dpi or higher is desirable for a reasonable shape evaluation. Please see the supplementary files p. 5 and Fig. S 2 for more details.

In addition, the estimated height h_{est} was assumed to be as follows for this study:

$$h_{est} = \frac{m}{S\rho} \quad (4)$$

where h_{est} is the height of samples predicted from the actual mass when the shape of them is presumed as a column of the projected image. h_{est} was used to define the flatness evaluation index F as follows:

$$F = \frac{h_{est}}{\phi} \quad (5)$$

2.5. Verification of the accuracy of mass estimation based on 3D models

The mass was estimated for Fragment, Foam, Line, and Pellet; estimation for Film could not be performed because of the insufficient number of samples. The basic form of the model was the volume and ρ of ellipsoid, referring to Simon et al. (2018) recommended by GESAMP (2019). The equation of the 3D model surface in the Cartesian coordinate system (x , y , z) was defined as:

$$\left\{ \frac{x}{\frac{\phi_h}{2}} \right\}^2 + \left\{ \frac{y}{\frac{\phi_h}{2}} \right\}^2 + \left\{ \frac{z}{\frac{\phi_h}{2}} \right\}^2 = 1 \quad (6)$$

Here, the z -axis (ϕ_h) was set to a times the particle diameter (either ϕ_l , ϕ_s , or ϕ) that was most proportional to h_{est} . The coefficient a was set to the value that minimized the total error between the estimated mass and the actual mass. If the estimated volume of the model shown in Eq. (6) is V_{est} , the estimated mass M_{est} is:

$$M_{est} = V_{est}\rho = \frac{4}{3} \left(\frac{\phi_l}{2} \right) \left(\frac{\phi_s}{2} \right) \left(\frac{\phi_h}{2} \right) \pi \rho \quad (7)$$

In addition to this, the following three models α , β , and γ were used to estimate the mass, and the accuracy was also compared by

calculating the mass ratio P of each model.

α) Model of Cózar et al. (2014):

$$M_{\text{Cózar}} = 0.1\Phi_l^3\rho \quad (8)$$

where $M_{\text{Cózar}}$ is the mass estimated by a 3D model with rectangular prism that base is a square with Φ_l as its base and height are 0.1 times of Φ_l .

β) Model of Simon et al. (2018):

$$M_{\text{Simon}} = \frac{4}{3} \left(\frac{\Phi_l}{2} \right) \left(\frac{\Phi_s}{2} \right) \left(\frac{0.67\Phi_s}{2} \right) \pi \rho \quad (9)$$

where M_{Simon} is the mass estimated by a 3D model with ellipsoid that principal axes Φ_l , Φ_s , and $0.67\Phi_s$.

γ) Model of Isobe et al. (2019):

$$M_{\text{Isobe}} = \rho 0.4\Phi_l \left(\frac{\Phi_l}{2} \right)^2 \pi \quad (10)$$

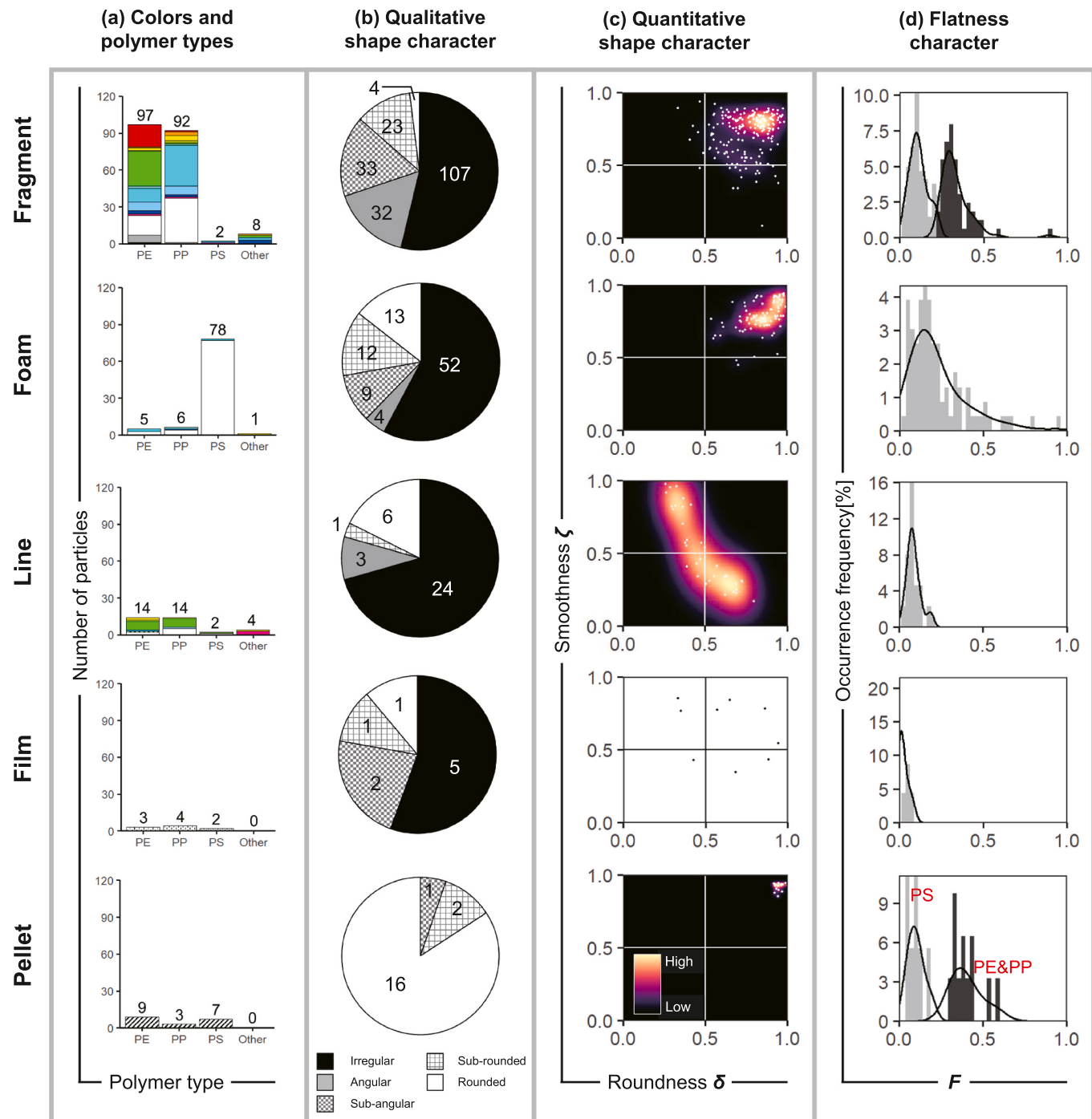


Fig. 2. Particle characteristic of each shape category. PE: polyethylene; PP: Polypropylene; PS: polystyrene; Other: other polymer type. (a): Number of pieces for each shape and for each composition. The color of the bars indicates the color of the particles. (b): Qualitative particle shape evaluation of each shape category sorted by Krumbein's roundness chart. (c): Scatter plots and distribution density heat maps for Roundness δ and Smoothness ζ . The brighter the color, the higher the distribution density. Film does not show heat map due to insufficient sample size. (d): Probability density function of F . The color in Fragment and Pellet indicate clusters by the k-means method. The dark gray belongs to the thick group and the light gray to the thin group.

where M_{Isobe} is the mass estimated by a 3D model with circle cylinder that base diameter is Φ_l and height is $0.4\Phi_l$.

The accuracy of the estimation of M was verified by calculating the ratio P between M and the actual mass (m) of the particles:

$$P_k = \frac{M_k}{m}, \quad (k = est, C\ddot{o}zar, Simon, Isobe) \quad (11)$$

2.6. Validation of the mass estimated by developed 3D models

The created 3D models were applied to a sample of another sandy beach facing Tokyo Bay to compare the estimated mass by the model with the actual mass. The samples were collected on January 29, 2021, at Kasai-Rinkai-Park West Beach ($35^{\circ}38'18.8''N$ $139^{\circ}51'20.2''E$, Tokyo Bay, Japan) and Makuhari Beach ($35^{\circ}38'36.4''N$ $140^{\circ}01'46.2''E$, Tokyo Bay, Japan, Fig. 1). Sample collection and pretreatment methods were the same as in section 2.1 and 2.2, but since the number of Line and PS-Pellet was small, the number of samples for each shape was adjusted to be at least three. The total estimated and actual masses and their ratios were calculated for each model.

Besides, all statistical processing was performed using R (R version 4.0.3).

3. Results

3.1. Handling validation

Comparison of the micrographs and binarization images of the particles before and after chemical treatment revealed minor differences in the direction of the protrusions on the particle contours, without any dissolution or disappearance in the particles (Fig. S 3). The brown stains were removed by chemical treatments. The mass of most of the particles did not change significantly, except for polystyrene (PS) particles, whose mass decreased to 84.8% of original mass (Fig. S 3). The relatively large decrease in PS was attributed to the fact that the surface structure of the Foam, which is the most common shape of PS (Fig. 2a), is complex and, therefore, favor the adhesion of organic matter and sand grains (Weinstein et al., 2016).

3.2. Particle shape, color, and polymer type

The number of particles used in the sample for each shape is shown in Fig. 2a. The most common shape was Fragment (199 items), which accounted for 57% of the total, followed by Foam (90 items, 26%), Line (34 items, 10%), Pellet (19 items, 5%), and Film (9 items, 2%). The most common color was White (173 items, 41%), followed by Cyan (51 items, 15%) and Green (46 items, 13%). All Films were Clear, and all Pellet particles were Opaque. The most common polymer type was polyethylene (PE, 129 items, 37%), followed by polypropylene (PP, 118 items, 34%) and polystyrene (PS, 91 items, 26%). Other polymer types were polyvinyl chloride (PVC, 4 items), butadiene rubber (BR, 3 items), polyvinyl acetate (PVAc, 2 items), polyamide-6 (PA-6, 1 item), poly methyl 2-methylpropenoate (PMMA, 1 item), polyurethane (PUR, 1 item), and styrene-butadiene rubber (SBR, 1 item).

3.3. Qualitative evaluation of particle shape

The classification results for each shape are shown in Fig. 2b. With the exception of Pellet, irregular was the most common among the four shapes (188 items, or 54% of the total 351 particles). Microplastics consisted of many irregular particles that were beyond the scope of classification by existing classification criteria. Especially for Line, Irregular accounted for the largest percentage (24 items, 71%) compared to other shapes and was found to be more irregular. On the other hand, Pellet had the highest percentage of Rounded shape (16 items, 84%).

3.4. Roundness δ and smoothness ζ of particles

The quantitative shape characteristics of whole particles were $\delta = 0.80 \pm 0.23$ (the numbers after \pm indicate the quartile deviation, same as after) and $\zeta = 0.78 \pm 0.18$. The distributions of δ and ζ for each shape are shown in Fig. 2c. 89% of Fragment, 98% of Foam, and 100% of Pellet categories were distributed in the range of ellipse and smooth surface with both δ and ζ greater than 0.50. In contrast, Line particles could be divided in smooth bar (47%) and rough elliptical (41%) shapes. The remaining 11% were distributed in the rough bar shapes.

3.5. Height of particles

The correlation between h_{est} and Φ_b , Φ_s , and Φ is shown in Table S 2. The particle diameter related to the estimated height was different for each shape, and h_{est} was significantly correlated with Φ_s for Fragment ($p < 0.001$), Φ for Foam and Line (Foam: $p = 0.08$, Line: $p < 0.05$), and Φ_l for Film and Pellet (Film: $p < 0.05$, Pellet: $p < 0.05$). (Film: $p < 0.05$, Pellet: $p < 0.05$). The probability density function of F for each shape is shown in Fig. 2d. The total shape conjectured to be flattened, with a long distribution on the right side, $F = 0.14 \pm 0.19$. As for shape, Fragment and Pellet had two peaks, which were divided into two groups by non-hierarchical clustering using the k-means method (the clustering results are shown in dark gray and light gray in Fig. 2d). Line and Film had low values for height (Line: $F = 0.09 \pm 0.15$, Film: $F = 0.03 \pm 0.03$) and had flattened shape.

The color and polymer type of particles in each group classified by F in Fragment (Fig. 3a) showed that red PE (15 items are thick, $n = 18$, Fig. 3a(i)) was predominantly classified into thick group ($F = 0.35 \pm 0.04$), whereas green PE (26 items are thin, $n = 28$, Fig. 3a(ii)) and cyan PP (26 items are thin, $n = 33$, Fig. 3a(iii)) were predominantly classified into thin group ($F = 0.11 \pm 0.03$). Detailed microscopic observation of these particles revealed that only the green PE (Fig. 3b(ii)) showed regularity in particle shape, and the cross-sectional shapes in the horizontal and vertical planes were all semi-elliptical with a radius of about 0.67 ± 0.11 mm and a fingertip-like shape with cracks in the same direction as Φ_s . In this study, the Green-PE in the Fragment (Green-PE-Fragment) was treated separately from the other particles as a half-elliptical particle in cross section. On the other hand, the other two particles did not show any shape regularity. From these points, although it is clear that there are two types of Fragment thicknesses, it was not possible to determine the thickness from the image or the polymer type of particles.

The scatter plot of F and Φ for Pellet (Fig. 3c) shows the cluster classification (■: thin group, ▲: thick group), in which PE and PP were clearly classified into the thick and large group ($F = 0.40 \pm 0.05$), while PS was clearly classified into the thin and flat group ($F = 0.10 \pm 0.03$).

3.6. Overview of the created models

For the Fragment, Foam, Line, and Pellet, ellipsoid models (Fig. 4a left) were created. Based on the results of 3.5 Height characteristics, the values used for z-axis Φ_h are determined. Fragment was found to have two types of height in the shape evaluation, but since it was not possible to classify the thickness of particles in terms of color and polymer type, the z-axis was set to only one direction, $3.72 \times 10^{-1} \Phi_s$. The Foam and Line values were $2.86 \times 10^{-1} \Phi$ and $1.31 \times 10^{-1} \Phi$. For Pellet, since the thickness of particles could be classified according to the polymer type, there were two ways: $1.43 \times 10^{-1} \Phi_l$ (PS-Pellet) and $5.65 \times 10^{-1} \Phi_l$ (PE/PP-Pellet). However, for the Green-PE-Fragment a separate 3D model of the semi-ellipsoid was created (Fig. 4a right). The z-axis of this model is set to 0.67 mm, and the estimated mass M_{est} is:

$$M_{est} = \frac{2}{3} \left(\frac{\Phi_l}{2} \right) \left(\frac{\Phi_s}{2} \right) \left(\frac{0.067}{2} \right) \pi \rho \quad (12)$$

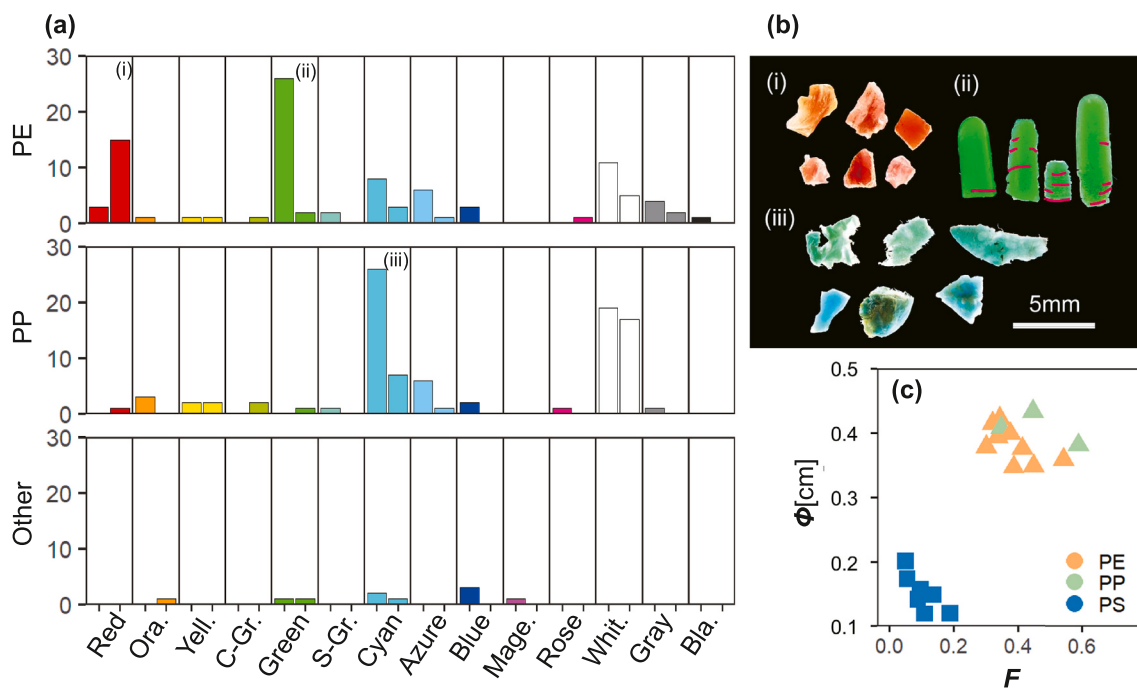


Fig. 3. Overview of clustering results for flatness (F) of Fragment and Pellet categories. (a): Number of particles categorized by both color and polymer types in Fragment. The left bars indicate thin and the right bars the thick particles from F cluster of Fig. 2d. The categories of each color are indicated at the bottom. Ora.: orange; Yell.: yellow; C-Gr.: chartreuse green; S-Gr.: spring green; Mage.: magenta; Whit.: white; Bla.: black. (b): Micrographs of (i)Red-PE, (ii)Green-PE, and (iii) Cyan-PE of the dominant categories in (a). The red lines on Green-PE particles (ii) indicates cracks. (c): Scatterplot of F and particle diameter (Φ) in Pellet category from F cluster of Fig. 2d. Squares represent the thin group and triangles the thick group. (For interpretation of the references to color in this figure legend, the reader is referred to the web version of this article.)

3.7. Verification of estimation accuracy of 3D model mass

The mass ratio P , for each model created and for models from other studies are shown in Fig. 4b and Table S 3. The results of the signed rank sum test between the actual and estimated masses of the particles are shown in Table S 4. The Shapiro-Wilk test showed no normality form in $m M_{est}$, M_{cozar} , M_{Simon} , and M_{Isobe} ($p < 0.001$). The model created in this study had a mass ratio closer to 1 than the other models for all shapes ($P_{est} = 1.06 \pm 0.84$), and there was no significant difference in mass from the original particles for all shapes except the Line shape ($p > 0.05$, Table S 4). The estimation error by model was smaller in the order $P_{est} > P_{Simon} (2.00 \pm 1.79) \geq P_{cozar} (1.58 \pm 3.72) > P_{Isobe} (4.94 \pm 1.17 \times 10)$. The P_{est} by shape was 1.11 ± 1.15 for Fragment (excluding Green-PE), 1.02 ± 0.27 for Green-PE-Fragment, 1.04 ± 0.97 for Foam, 1.09 ± 0.48 for Line (but with a significant difference, $p = 0.012$), 1.04 ± 0.29 for PE/PP-Pellet, and 1.02 ± 0.58 for PS-Pellet. The PE/PP-Pellet was 1.04 ± 0.29 , and the PS-Pellet was 1.02 ± 0.58 . On the other hand, the models of other studies, Foam and PS-Pellet for M_{cozar} and PE/PP-Pellet for M_{Simon} and M_{Isobe} , were not significantly different from m . In Line, the models of M_{cozar} and M_{Isobe} which used only the primary axis, produced relatively large estimation errors, $P_{cozar} = 1.42 \times 10 \pm 1.79 \times 10$ and $P_{Isobe} = 4.47 \times 10 \pm 5.63 \times 10$, respectively. Fig. 4c and d shows the relationship between δ and ζ , and the mass ratio of each model. P_{cozar} and P_{Isobe} tended to have significantly larger mass ratios as δ became smaller, resulting in an overestimation of the estimated mass, while P_{est} and P_{Simon} tended to have significantly larger mass ratios as ζ became smaller.

3.8. Validation of the created 3D model mass

Estimation of the mass of particles in other regions by the model developed using samples from the Tsurumi River estuary revealed that the total estimated mass was 1.03 times the actual mass (Table S 5). By

this model, a slight overestimation was found in the range of 0.9 to 1.3 times the actual mass for all shapes except Fragment (including Green-PE-Fragment). The highest overestimation was observed for PS-Pellet (1.3 times), followed by Line (1.27 times).

4. Discussion

The impacts caused by microplastics in marine organisms that were reported in the last years (Anbumani and Kakkar, 2018; Wright et al., 2013) have increased the need to better classify and assess their abundance in marine environments. In this study, the analysis of microplastics collected in an estuarine area of a river that crosses a densely populated area in Japan revealed a wide diversity in shape, polymer types, and color with some trends in specific categories and in terms of abundance. In the mass estimation model using 3D, it was possible to significantly improve the accuracy for all categories of microplastics analyzed.

The analysis of particle from the estuary of Tsurumi River revealed that the most common microplastic was of Fragment type (57%), composed by PE or PP, with white, cyan, and green colors. The category foam (26%) was composed mainly by PS and had white color. The third most common was Line category (10%), composed by PE or PP, with green color. This trend was similar to other survey in Japan (Nakano et al., 2021), though survey area is different from our sampling point. The evaluation of shape of microplastics suggested that microplastics are more complex and diverse than the range of shapes that have been assumed for particles. In general, microplastics were slender ($\delta = 0.8 \pm 0.23$), had irregular contours ($\zeta = 0.78 \pm 0.18$), and had flat plate-like shapes ($F = 0.14 \pm 0.19$). This trend is almost the same as that of Simon et al. (2018), where the short diameter was 67% of the long diameter. The irregularity of each shape tends to be closer to spherical shape in the order of Pellet > Foam > Fragment > Line, which is similar to generalizations proposed by Kooi and Koelmans (2019). But, with the exception for Pellet, the height of particles was overestimated in their

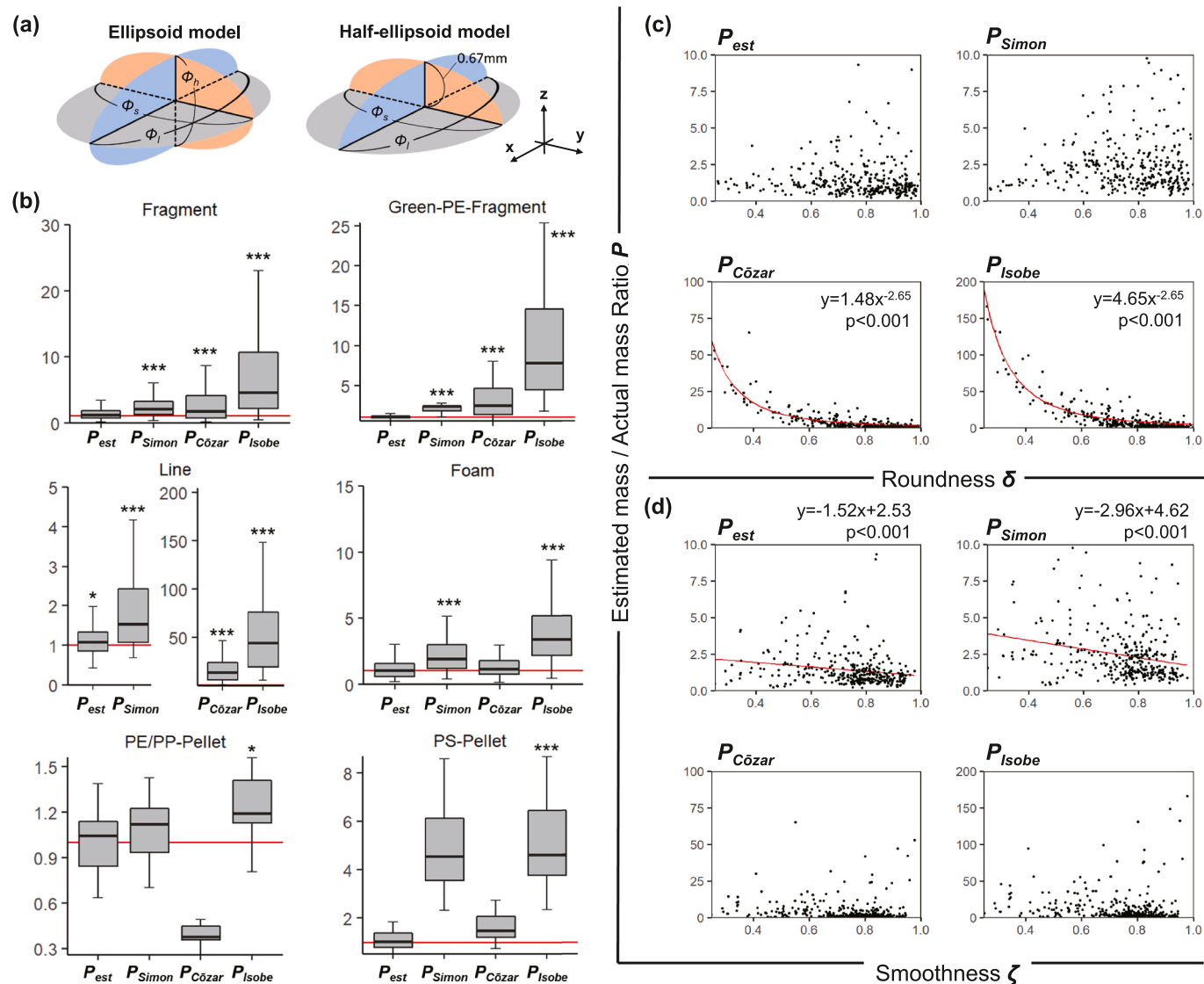


Fig. 4. Overview of mass estimation using 3D models. (a): Conceptual figure of the models created in this study. ϕ_l : major axis of the approximate ellipse; ϕ_s minor axis of the approximate ellipse. Left: Ellipsoid models in Fragment, Foam, Line and Pellet. Right: Half of ellipsoid model in Green-PE-Fragment (Artificial grass). (b): Box plots of estimated mass and actual mass ratio for each 3D model. The red Line indicates mean ratio = 1. Asterisks indicate p -values for the signed rank sum test with particle mass, ***: $p < 0.001$; *: $p < 0.05$. Estimation error for models considering Roundness δ (c) and Smoothness ζ (d). (For interpretation of the references to color in this figure legend, the reader is referred to the web version of this article.)

models and for this reason they need to be improved. In this context, the detailed characterization of particles at a given location, including other information such as height, can contribute to improve the efficacy of mass estimation methods (see discussion below).

In our 3D ellipsoid and half-ellipsoid models, that incorporate slenderness and height parameters, a higher estimation accuracy was obtained compared to other models that do not consider or consider only one of these parameters. The rectangular (Cózar et al., 2014) and circular cylinder (Isobe et al., 2019) models that used only long diameters failed to account for the slenderness of the particles, showing overestimations that increased proportionally with slenderness, and consequently low accuracy values (1.58 ± 3.72 , 4.94 ± 11.71 , respectively). Compared to the ellipsoid model that incorporates slenderness (Simon et al., 2018), the inclusion of height (our model) improved significantly the accuracy (1.06 ± 0.84 , 2.00 ± 1.79 , respectively) of mass estimation, suggesting that the addition of specific parameters can contribute to improve the approximation capacity of particles actual mass using 3D models.

The poor accuracy of mass estimation for Line, which was the lowest

among the five categories of microplastics analyzed by our 3D model, relies on the complexity related to shape. This is because instead of a bar-like, simple structure, 41% of the particles were quantitatively evaluated as “ellipse with rough surface”. For a straight Line (Fig. 5a-2, 3, 5, 9, 10), the approximate ellipse has a slender shape (Fig. 5b), which reflects the original structure. In contrast, in the bent Line (Fig. 5a-1, 4, 6, 7, 8), the approximate ellipse is closer to a circle and does not represent properly its slenderness (Fig. 5b). However, since the original particle and the approximate ellipse have the same area, the original perimeter is relatively longer than that of the approximate ellipse, and the shape is evaluated as having a larger δ and a smaller ζ . As a result, the slenderness of the bent Line is expressed as an irregularity, and the evaluation does not reflect the original shape. These points illustrate the limitations for a correct evaluation of microplastics shape and, hence, new strategies need to be developed.

The green microplastics represented about 14% of the total number of Fragment category and were mainly composed by PE, similarly to the results from a previous study at Tokyo Bay (Nakano et al., 2021). The estimation of mass performed in these fragments, that may comprise

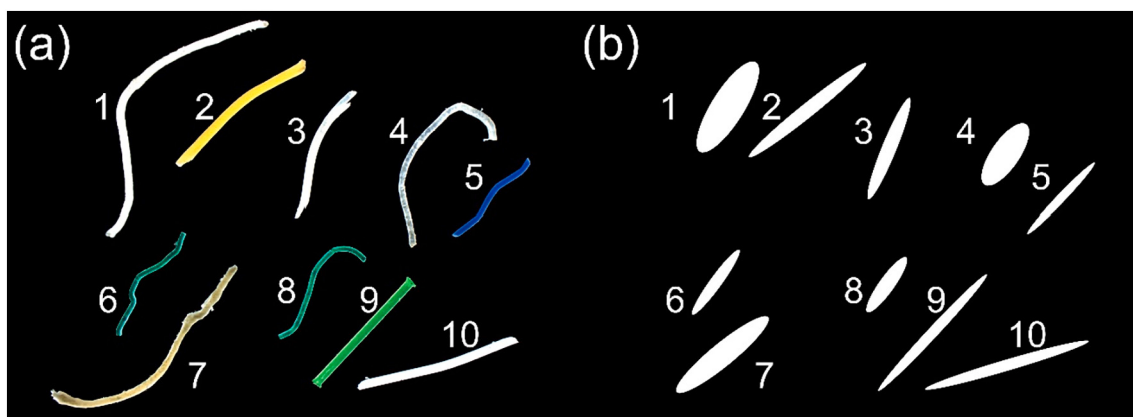


Fig. 5. Comparison of shapes obtained by image analysis for Line category. Real microscopic image (a) and the respective approximate ellipse image (b).

pieces of artificial grass based on their color and shape, using a dedicated half-ellipsoid model resulted in a higher accuracy ($P_{est} = 1.02 \pm 0.27$) compared to other studies (Cózar et al., 2014; Isobe et al., 2019; Simon et al., 2018) and other shapes (our models). The use of dedicated models for specific types of particles, such as artificial grass, that are characteristic in some regions can be an efficient strategy for optimizing mass estimation of microplastics. Also, as exemplified by the artificial grass, features related to shape, color, and polymer type can have some sort of correlation and thus be very useful for obtaining information about the source of microplastics (GESAMP, 2019). In case of Europe, 98.7% of beach microplastics belong to Line category and 70–90% have blue or black color (Lots et al., 2017), indicating the existence of some regularities in abundance of particles according to regions and environments. Those information on features and abundance of microplastics, together with identification of trends in samples from different sources may allow the employment of dedicated models for optimized and large-scale mass estimation.

The validation of the estimated masses by the developed model showed good results with a total of 1.03 times the actual mass, suggesting that the obtained particle shapes are universally applicable in Tokyo Bay from a macroscopic point of view. On the other hand, Line and PS-Pellet were relatively overestimated in comparison to the other shapes. The reason for the decrease in the estimation accuracy of Line may be due to the evaluation method, as mentioned above, but also due to the small number of particles in Tokyo Bay. PS-Pellet is classified as Pellet by GESAMP (2019), but it is thought to have a sponge structure. On the other hand, the surface structure of styrene foam type microplastics is known to be scaly, which means that the structure may be destroyed and shrunk by mechanical erosion by sands, UV light and biological degradation in the environment (Zhou et al., 2018). Therefore, PS-Pellet that drifted to the beach through the process of drift, such as samples from Kasai-Rinkai-Park and Makuhari, is considered to have shrunk more than those that were just released into the environment in the estuary. This kind of error seems to be a limitation of mass estimation by simple image analysis. While mass estimation by image analysis has the merit of being simple and can be quickly applied to previous research, additional innovations are needed for more precise mass quantification. Consideration of the carbonyl index in the infrared absorption spectrum, which is an indicator of particle degradation (Prata et al., 2020), detailed understanding of shape using quantitative phase imaging (QPI) and holographic techniques (Bianco et al., 2020; Cacace et al., 2020; Nayak et al., 2021; Takahashi et al., 2020), depth estimation of particle images using deep learning (Garg et al., 2016; Rajagopalan et al., 2004), further understanding of particle structure using multi-resolution and multivariate image analysis (Facco et al., 2009), and mass quantification using pyr-GC/MS (Dierkes et al., 2019; Funck et al., 2020; Peters et al., 2018) may lead to solutions to these issues, though the operation may possibly involve complex analysis.

In marine organisms, the features of microplastics can have implications on the biological impacts. For instance, there is a concern that the irregular shape of the particles leads to an increase in surface area, which in turn may increase the adsorption of harmful hydrophobic substances, such as polychlorinated biphenyls (PCBs), by the organisms. In rearing experiments, irregular particles stay longer in the digestive tract than simple particles, causing prolonged digestive inhibition (Au et al., 2015; Frydkjær et al., 2017). In case of colors, it is possible that bright colors of microplastics increase the risk of uptake by organisms that use visual information for foraging. It was demonstrated that the Japanese sea perch *Lateolabrax japonicus* recognize white or green objects as their prey (Okamoto et al., 2001), and these colors were very common in our samples. Although the complexity and color of the particles have not yet been taken into account in generalized models of microplastics (Kooi and Koelmans, 2019), these examples indicate that these visual aspects can leverage the impacts on marine organisms.

5. Conclusion

The standardization of microplastic quantification is important for measuring the abundance and to evaluate the impacts of marine pollution on marine ecosystems. We first conducted a direct shape evaluation analysis that revealed that the microplastics are mostly plate-like particles; a regular shape that was abundant in our samples called “artificial grass” was also identified. Then, we measured the mass of each particle using 3D models, incorporating slenderness and height parameters, and obtained a more accurate picture of the mass for most of shape categories, except for Line. The use of a dedicated model for artificial grass allowed us to improve the estimation accuracy. From these points, we conclude that the inclusion of shape characteristics in a 3D model-based mass estimation method is very efficient to access the mass of microplastics with high precision.

Funding

This study was supported by the Environmental Research and Technology Development Fund (JPMEERF18S20208) of the Ministry of the Environment, Japan.

CRediT authorship contribution statement

Hiraku Tanoiri: Conceptualization, Formal analysis, Investigation, Writing – original draft. **Haruka Nakano:** Methodology, Validation, Writing – review & editing. **Hisayuki Arakawa:** Project administration, Resources, Validation, Writing – review & editing. **Ricardo Shohei Hattori:** Validation, Visualization, Writing – review & editing. **Masashi Yokota:** Supervision, Writing – review & editing.

Declaration of competing interest

The authors declare that they have no known competing financial interests or personal relationships that could have appeared to influence the work reported in this paper.

Acknowledgements

We would like to express our gratitude to Dr. Carlos A. Strüssmann and Dr. Yoji Yamamoto for their helpful advice. We are also indebted to Mr. Sota Takahashi for support with sample collection.

Appendix A. Supplementary data

Supplementary data to this article can be found online at <https://doi.org/10.1016/j.marpolbul.2021.112749>.

References

- Anbumani, S., Kakkar, P., 2018. Ecotoxicological effects of microplastics on biota: a review. *Environ. Sci. Pollut. Res.* <https://doi.org/10.1007/s11356-018-1999-x>.
- Association of Plastics Manufacturers, 2018. Plastics -The facts 2018. *Plast. Eur.*
- Au, S.Y., Bruce, T.F., Bridges, W.C., Klaine, S.J., 2015. Responses of *Hyalella azteca* to acute and chronic microplastic exposures. *Environ. Toxicol. Chem.* <https://doi.org/10.1002/etc.3093>.
- Barnes, D.K.A., Galgani, F., Thompson, R.C., Barlaz, M., 2009. Accumulation and fragmentation of plastic debris in global environments. *Philos. Trans. R. Soc. B Biol. Sci.* <https://doi.org/10.1098/rstb.2008.0205>.
- Besseling, E., Wegner, A., Foekema, E.M., Van Den Heuvel-Greve, M.J., Koelmans, A.A., 2013. Effects of microplastic on fitness and PCB bioaccumulation by the lugworm *Arenicola marina* (L.). *Environ. Sci. Technol.* <https://doi.org/10.1021/es302763x>.
- Bianco, V., Memmolo, P., Carcagni, P., Merola, F., Paturzo, M., Distante, C., Ferraro, P., 2020. Microplastic identification via holographic imaging and machine learning. *Adv. Intell. Syst.* 2, 1900153. <https://doi.org/10.1002/aisy.201900153>.
- Blott, S.J., Pye, K., 2008. Particle shape: a review and new methods of characterization and classification. *Sedimentology*. <https://doi.org/10.1111/j.1365-3091.2007.00892.x>.
- Cacace, T., Bianco, V., Mandracchia, B., Pagliarulo, V., Oleandro, E., Paturzo, M., Ferraro, P., 2020. Compact off-axis holographic slide microscope: design guidelines. *Biomed. Opt. Express* 11, 2511. <https://doi.org/10.1364/boe.11.002511>.
- Claessens, M., Van Cauwenbergh, L., Vandegheuchte, M.B., Janssen, C.R., 2013. New techniques for the detection of microplastics in sediments and field collected organisms. *Mar. Pollut. Bull.* <https://doi.org/10.1016/j.marpolbul.2013.03.009>.
- Corami, F., Rosso, B., Bravo, B., Gambaro, A., Barbante, C., 2020. A novel method for purification, quantitative analysis and characterization of microplastic fibers using micro-FTIR. *Chemosphere*. <https://doi.org/10.1016/j.chemosphere.2019.124564>.
- Cózar, A., Echevarría, F., González-Gordillo, J.I., Irigoien, X., Úbeda, B., Hernández-León, S., Palma, Á.T., Navarro, S., García-de-Lomas, J., Ruiz, A., Fernández-de-Puelles, M.L., Duarte, C.M., 2014. Plastic debris in the open ocean. *Proc. Natl. Acad. Sci. U. S. A.* 111, 10239–10244. <https://doi.org/10.1073/pnas.1314705111>.
- Davidson, K., Dudas, S.E., 2016. Microplastic Ingestion by Wild and Cultured Manila Clams (*Venerupis philippinarum*) from Baynes Sound, British Columbia. *Arch. Environ. Contam. Toxicol.* <https://doi.org/10.1007/s00244-016-0286-4>.
- Dehaut, A., Cassone, A.L., Frère, L., Hermabessiere, L., Himber, C., Rinnert, E., Rivière, G., Lambert, C., Soudant, P., Huvet, A., Duflos, G., Paul-Pont, I., 2016. Microplastics in seafood: Benchmark protocol for their extraction and characterization. *Environ. Pollut.* <https://doi.org/10.1016/j.envpol.2016.05.018>.
- Dierkes, G., Lauschke, T., Becher, S., Schumacher, H., Földi, C., Ternes, T., 2019. Quantification of microplastics in environmental samples via pressurized liquid extraction and pyrolysis-gas chromatography. *Anal. Bioanal. Chem.* <https://doi.org/10.1007/s00216-019-02066-9>.
- Eisma, D., 1991. Particle size of suspended matter in estuaries. *Geo-Marine Lett.* 11, 147–153.
- Enders, K., Lenz, R., Beer, S., Stedmon, C.A., 2017. Extraction of microplastic from biota: Recommended acidic digestion destroys common plastic polymers. *ICES J. Mar. Sci.* <https://doi.org/10.1093/icesjms/fsw173>.
- Facco, P., Bezzo, F., Barolo, M., Mukherjee, R., Romagnoli, J.A., 2009. Monitoring roughness and edge shape on semiconductors through multiresolution and multivariate image analysis. *AIChE J.* 55, 1147–1160. <https://doi.org/10.1002/ai.11733>.
- Frydkjær, C.K., Iversen, N., Roslev, P., 2017. Ingestion and egestion of microplastics by the cladoceran *Daphnia magna*: effects of regular and irregular shaped plastic and sorbed phenanthrene. *Bull. Environ. Contam. Toxicol.* <https://doi.org/10.1007/s00128-017-2186-3>.
- Funck, M., Yildirim, A., Nickel, C., Schram, J., Schmidt, T.C., Tuerk, J., 2020. Identification of microplastics in wastewater after cascade filtration using pyrolysis-GC-MS. *MethodsX*. <https://doi.org/10.1016/j.mex.2019.100778>.
- Garg, R., Vijay Kumar, B.G., Carneiro, G., Reid, I., 2016. Unsupervised CNN for single view depth estimation: geometry to the rescue. In: Lecture Notes in Computer Science (Including Subseries Lecture Notes in Artificial Intelligence and Lecture Notes in Bioinformatics). https://doi.org/10.1007/978-3-319-46484-8_45.
- GESAMP, 2019. Guidelines for the monitoring and assessment of plastic litter in the ocean. In: GESAMP Reports & Studies Series.
- Horton, A.A., Dixon, S.J., 2018. Microplastics: An introduction to environmental transport processes. *Wiley Interdiscip. Rev. Water.* <https://doi.org/10.1002/wat2.1268>.
- Isobe, A., Iwasaki, S., Uchida, K., Tokai, T., 2019. Abundance of non-conservative microplastics in the upper ocean from 1957 to 2066. *Nat. Commun.* <https://doi.org/10.1038/s41467-019-108316-9>.
- Ivar Do Sul, J.A., Costa, M.F., 2014. The present and future of microplastic pollution in the marine environment. *Environ. Pollut.* <https://doi.org/10.1016/j.envpol.2013.10.036>.
- Jambeck, J.R., Geyer, R., Wilcox, C., Siegler, T.R., Perryman, M., Andrade, A., Narayan, R., Law, K.L., 2015. Plastic waste inputs from land into the ocean. *Science.* <https://doi.org/10.1126/science.1260352>.
- Kataoka, T., Nihei, Y., Kudou, K., Hinata, H., 2019. Assessment of the sources and inflow processes of microplastics in the river environments of Japan. *Environ. Pollut.* 244, 958–965. <https://doi.org/10.1016/j.envpol.2018.10.111>.
- Kooi, M., Koelmans, A.A., 2019. Simplifying microplastic via continuous probability distributions for size, shape, and density. *Sci. Technol. Lett. Environ.* <https://doi.org/10.1021/acs.estlett.9b00379>.
- Krumbein, W.C., 1941. Measurement and geological significance of shape and roundness of sedimentary particles. *SEPM J. Sediment. Res.* <https://doi.org/10.1306/d42690f3-2b26-11d7-8648000102c1865d>.
- Lebreton, L.C.M., Van Der Zwart, J., Damsteeg, J.W., Slat, B., Andrade, A., Reisser, J., 2017. River plastic emissions to the world's oceans. *Nat. Commun.* <https://doi.org/10.1038/ncomms15611>.
- Lots, F.A.E., Behrens, P., Vijver, M.G., Horton, A.A., Bosker, T., 2017. A large-scale investigation of microplastic contamination: abundance and characteristics of microplastics in European beach sediment. *Mar. Pollut. Bull.* <https://doi.org/10.1016/j.marpolbul.2017.08.057>.
- MLITJapan, 2010. Area, total population, and general assets of watersheds, etc. in first-class water systems (watersheds) [WWW Document]. <https://www.mlit.go.jp/common/001184133.pdf>.
- Munno, K., Helm, P.A., Jackson, D.A., Rochman, C., Sims, A., 2018. Impacts of temperature and selected chemical digestion methods on microplastic particles. *Environ. Toxicol. Chem.* <https://doi.org/10.1002/etc.3935>.
- Nakano, H., Arakawa, H., Tokai, T., 2021. Microplastics on the sea surface of the semi-closed Tokyo Bay. *Mar. Pollut. Bull.* 162, 111887. <https://doi.org/10.1016/j.marpolbul.2020.111887>.
- Nayak, A.R., Malkiel, E., McFarland, M.N., Twardowski, M.S., Sullivan, J.M., 2021. A review of holography in the aquatic sciences: in situ characterization of particles, plankton, and small scale biophysical interactions. *Front. Mar. Sci.* 7, 1–16. <https://doi.org/10.3389/fmars.2020.572147>.
- Okamoto, M., Kawamura, G., Tanaka, Y., 2001. Selectivity of color of lure by Japanese sea bass *Lateolabrax japonicus* under different background colors. *Nippon Suisan Gakkaishi.* <https://doi.org/10.2331/suisan.67.449>.
- Oliveira, M., Ribeiro, A., Hylland, K., Guilhermino, L., 2013. Single and combined effects of microplastics and pyrene on juveniles (0+ group) of the common goby *Pomatoschistus microps* (Teleostei, Gobiidae). *Ecol. Indic.* <https://doi.org/10.1016/j.ecolind.2013.06.019>.
- Pan, Z., Guo, H., Chen, H., Wang, S., Sun, X., Zou, Q., Zhang, Y., Lin, H., Cai, S., Huang, J., 2019. Microplastics in the Northwestern Pacific: Abundance, distribution, and characteristics. *Sci. Total Environ.* <https://doi.org/10.1016/j.scitotenv.2018.09.244>.
- Peters, C.A., Hendrickson, E., Minor, E.C., Schreiner, K., Halbur, J., Brattton, S.P., 2018. Pyr-GC/MS analysis of microplastics extracted from the stomach content of benthivore fish from the Texas Gulf Coast. *Mar. Pollut. Bull.* <https://doi.org/10.1016/j.marpolbul.2018.09.049>.
- Prata, J.C., Reis, V., Paço, A., Martins, P., Cruz, A., da Costa, J.P., Duarte, A.C., Rocha-Santos, T., 2020. Effects of spatial and seasonal factors on the characteristics and carbonyl index of (micro)plastics in a sandy beach in Aveiro, Portugal. *Sci. Total Environ.* 709 <https://doi.org/10.1016/j.scitotenv.2019.135892>.
- Primpke, S., Cross, R.K., Mintenig, S.M., Simon, M., Vianello, A., Gerdts, G., Vollertsen, J., 2020a. Toward the Systematic Identification of Microplastics in the Environment: Evaluation of a New Independent Software Tool (siMPle) for Spectroscopic Analysis. *Appl. Spectrosc.* 74, 1127–1138. <https://doi.org/10.1177/0003702820917760>.
- Primpke, S., Fischer, M., Lorenz, C., Gerdts, G., Scholz-Böttcher, B.M., 2020b. Comparison of pyrolysis gas chromatography/mass spectrometry and hyperspectral FTIR imaging spectroscopy for the analysis of microplastics. *Anal. Bioanal. Chem.* 412, 8283–8298. <https://doi.org/10.1007/s00216-020-02979-w>.
- Qu, X., Su, L., Li, H., Liang, M., Shi, H., 2018. Assessing the relationship between the abundance and properties of microplastics in water and in mussels. *Sci. Total Environ.* <https://doi.org/10.1016/j.scitotenv.2017.11.284>.
- Rajagopalan, A.N., Chaudhuri, S., Mudenanagudi, U., 2004. Depth estimation and image restoration using defocused stereo pairs. *IEEE Trans. Pattern Anal. Mach. Intell.* <https://doi.org/10.1109/TPAMI.2004.102>.
- Rocha-Santos, T., Duarte, A.C., 2015. A critical overview of the analytical approaches to the occurrence, the fate and the behavior of microplastics in the environment. *TrAC - Trends Anal. Chem.* <https://doi.org/10.1016/j.trac.2014.10.011>.
- Siegfried, M., Koelmans, A.A., Besseling, E., Kroese, C., 2017. Export of microplastics from land to sea. A modelling approach. *Water Res.* <https://doi.org/10.1016/j.watres.2017.10.011>.

- Silva-Cavalcanti, J.S., Silva, J.D.B., de França, E.J., de Araújo, M.C.B., Gusmão, F., 2017. Microplastics ingestion by a common tropical freshwater fishing resource. Environ. Pollut. <https://doi.org/10.1016/j.envpol.2016.11.068>.
- Simon, M., van Aist, N., Vollerstsen, J., 2018. Quantification of microplastic mass and removal rates at wastewater treatment plants applying focal plane array (FPA)-based Fourier transform infrared (FT-IR) imaging. Water Res. <https://doi.org/10.1016/j.watres.2018.05.019>.
- Sugimoto, M., Yokota, N., Nakazawa, H., 1989. Characterization of a particle by a pair of shape indexes. J. Soc. Powder Technol. Japan. <https://doi.org/10.4164/sptj.26.624>.
- Sussarellu, R., Suquet, M., Thomas, Y., Lambert, C., Fabiou, C., Pernet, M.E.J., Goïc, N., Le, Quillien, V., Mingant, C., Epelboin, Y., Corporeau, C., Guyomarch, J., Robbens, J., Paul-Pont, I., Soudant, P., Huvet, A., 2016. Oyster reproduction is affected by exposure to polystyrene microplastics. Proc. Natl. Acad. Sci. U. S. A. <https://doi.org/10.1073/pnas.1519019113>.
- Takahashi, T., Liu, Z., Thevar, T., Burns, N., Mahajan, S., Lindsay, D., Watson, J., Thornton, B., 2020. Identification of microplastics in a large water volume by integrated holography and Raman spectroscopy. Appl. Opt. 59, 5073. <https://doi.org/10.1364/ao.393643>.
- Takashimizu, Y., Iiyoshi, M., 2016. New parameter of roundness R: circularity corrected by aspect ratio. Prog. Earth Planet. Sci. <https://doi.org/10.1186/s40645-015-0078-x>.
- Uncles, R.J., Stephens, J.A., Harris, C., 2006. Properties of suspended sediment in the estuarine turbidity maximum of the highly turbid Humber Estuary system, UK. Ocean Dyn. 56, 235–247. <https://doi.org/10.1007/s10236-005-0053-y>.
- Ushijima, T., Tanaka, S., Suzuki, Y., Yukioka, S., Wang, M., Nabetani, Y., Fujii, S., Takada, H., 2018. Occurrence of microplastics in digestive tracts of fish with different modes of ingestion in Japanese bays and Lake Biwa. J. Japan Soc. Water Environ. <https://doi.org/10.2965/jswe.41.107>.
- Wang, S.D., Shen, Y.M., Guo, Y.K., Tang, J., 2008. Three-dimensional numerical simulation for transport of oil spills in seas. Ocean Eng. <https://doi.org/10.1016/j.oceaneng.2007.12.001>.
- Weinstein, J.E., Crocker, B.K., Gray, A.D., 2016. From macroplastic to microplastic: degradation of high-density polyethylene, polypropylene, and polystyrene in a salt marsh habitat. Environ. Toxicol. Chem. 35, 1632–1640. <https://doi.org/10.1002/etc.3432>.
- Wright, S.L., Thompson, R.C., Galloway, T.S., 2013. The physical impacts of microplastics on marine organisms: a review. Environ. Pollut. <https://doi.org/10.1016/j.envpol.2013.02.031>.
- Zhao, S., Zhu, L., Wang, T., Li, D., 2014. Suspended microplastics in the surface water of the Yangtze Estuary System, China: first observations on occurrence, distribution. Mar. Pollut. Bull. <https://doi.org/10.1016/j.marpolbul.2014.06.032>.
- Zhou, Q., Zhang, H., Fu, C., Zhou, Y., Dai, Z., Li, Y., Tu, C., Luo, Y., 2018. The distribution and morphology of microplastics in coastal soils adjacent to the Bohai Sea and the Yellow Sea. Geoderma 322, 201–208. <https://doi.org/10.1016/j.geoderma.2018.02.015>.